

# PCCP

Accepted Manuscript



This is an *Accepted Manuscript*, which has been through the Royal Society of Chemistry peer review process and has been accepted for publication.

*Accepted Manuscripts* are published online shortly after acceptance, before technical editing, formatting and proof reading. Using this free service, authors can make their results available to the community, in citable form, before we publish the edited article. We will replace this *Accepted Manuscript* with the edited and formatted *Advance Article* as soon as it is available.

You can find more information about *Accepted Manuscripts* in the [Information for Authors](#).

Please note that technical editing may introduce minor changes to the text and/or graphics, which may alter content. The journal's standard [Terms & Conditions](#) and the [Ethical guidelines](#) still apply. In no event shall the Royal Society of Chemistry be held responsible for any errors or omissions in this *Accepted Manuscript* or any consequences arising from the use of any information it contains.



Journal Name

ARTICLE

## TEMPO-mediated oxidized winter melon-based carbonaceous aerogel as an ultralight 3D support for enhanced photodegradation capacities of organic pollutants

Received 00th January 20xx,  
Accepted 00th January 20xx

DOI: 10.1039/x0xx00000x

www.rsc.org/

Miao Miao,<sup>a</sup> Gangling Wang,<sup>a</sup> Shaomei Cao,<sup>a</sup> Xin Feng,<sup>a\*</sup> Jianhui Fang<sup>b</sup> and Liyi Shi<sup>a</sup>

Natural biomass based carbonaceous aerogel is becoming a promising lightweight, biodegradable matrix to supersede traditional support materials in realizing future sustainable photochemistry and environment protection. Herein, flower-like BiOBr loaded onto an ultralight TEMPO-mediated oxidized carbonaceous aerogel (BOB@OWMCA) support was successfully prepared using the edible winter melon as source material via a simple solvothermal method. The three-dimensional sponge-like OWMCA with surface functionalization displayed ultralow density (17.7 mg/cm<sup>3</sup>) and large special surface area (30.6 m<sup>2</sup>/g). The BiOBr was homogeneously anchored on the surface of the hierarchical porous OWMCA exhibiting synergetic properties of BiOBr photocatalyst and OWMCA support for strengthening photodegradation capacities. The results indicated that the as-prepared BOB@OWMCA composite was demonstrated outstanding adsorption and photodegradation capacities for organic pollutants (rhodamine B) under visible light irradiation. Of importance here, BOB@OWMCA composite showed a prominent advantage for easy collection and separation from the aqueous system, making it a promising candidate as robust visible light responsive photocatalysts for the potential applications.

### Introduction

Semiconductor photocatalysts have attracted considerable attention in the past decades because of their wide potential application in environmental protection such as air purification, wastewater treatment and water splitting<sup>1-3</sup>. However, the conventionally used TiO<sub>2</sub> photocatalyst suffers from some drawbacks due to no light absorption under visible light region and the low quantum efficiency<sup>4</sup>. Bismuth-based oxyhalides (BiOX, X = Cl, Br or I) with unique layered structure have recently been evaluated to effectual non-TiO<sub>2</sub> photocatalysts showing remarkable photocatalytic activities and strong adsorption under ultraviolet (UV) or visible light irradiation<sup>4-6</sup>. BiOBr is of particular importance among the most active BiOX compounds for its suitable band gap, excellent stability and relatively superior visible light photocatalytic ability<sup>7</sup>. Recently, BiOBr with various architectures such as nanosheets<sup>7,8</sup>, microspheres<sup>9</sup>, mesoporous microspheres<sup>10</sup>, 3D flower-like nanoarchitectures<sup>11</sup>, and heterojunctions<sup>12,13</sup> have been

demonstrated for the enhancement of the photocatalytic ability. But the inherent difficulty to efficiently separate ultrafine particulate BiOBr from the aqueous systems hinders its practical applications<sup>14,15</sup>. Therefore, finding an ideal way to immobilize BiOBr photocatalysts on certain supports for easy collection and separation is still an urgent requirement. Several inert or active supports such as silica, zeolites, glass slides, Ti disk, Nafion membrane, activated carbon and graphitic carbon nitride were utilized to host granular nanocatalysts<sup>15-20</sup>. Li et al.<sup>15</sup> utilized Ti disk as a support to synthesize a double hierarchical structured BiOBr film exhibiting strong RhB adsorption capacity and high light utilization efficiency. Mitchell et al.<sup>16</sup> adopted a macroporous ZrO<sub>2</sub> support to fabricate the chemically inert photonic ZrO<sub>2</sub> decorated with CdS nanoparticles to increase the yield of hydrogen production. Cuellar et al.<sup>17</sup> used glass slides as substrates to prepare BiOBr thin films to eliminate the inconvenient of photocatalyst's removal from aqueous medium. Zhang et al.<sup>19,20</sup> applied g-C<sub>3</sub>N<sub>4</sub> sheets as good support to develop highly efficient hierarchical g-C<sub>3</sub>N<sub>4</sub>-based composite photocatalysts in environmental pollution cleanup. Recently, developments for cleaner, sustainable chemistry are being driven by environmentally friendly native biomaterials. Therefore, the three-dimensional (3D) carbon-based aerogel has been widely applied in solar cells<sup>21</sup>, various sensors<sup>22</sup>, batteries<sup>23-25</sup>, supercapacitors<sup>26</sup> and water purification<sup>29-29</sup>. Due to its low density, large specific surface area and high porosity, porous 3D carbon-based aerogel is becoming an important research object, which can be acted as an ideal

<sup>a</sup> Research Center of Nano Science and Technology, Shanghai University, Shanghai 200444, P. R. China. \*Corresponding Author: [fenqixin@shu.edu.cn](mailto:fenqixin@shu.edu.cn)

<sup>b</sup> Department of Chemistry, Shanghai University, Shanghai 200444, P. R. China.

Electronic Supplementary Information (ESI) available: [SEM images of WMCA and OWMCA in Figure S1; Photograph of the as-prepared OWMCA monoliths with different volumes in Figure S2; Photographs of the BOB@OWMCA monolith standing on the feathers in Figure S3; SEM image of flower-like BiOBr microspheres on the surface of OWMCA in Figure S4; Nitrogen adsorption-desorption isotherm of BOB@OWMCA composites with different ratios in Figure S5.]. See DOI: 10.1039/x0xx00000x

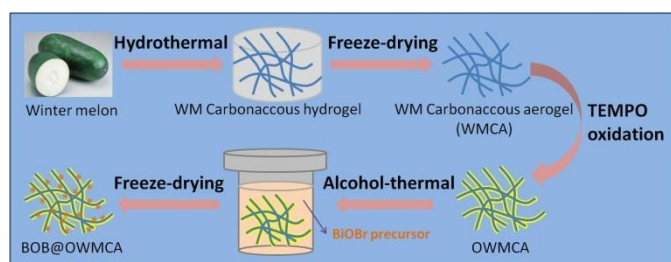
candidate support for the heterogeneous catalysts<sup>30-32</sup>. But the inherent surface hydrophobicity and lack of surface active groups of carbon materials hinder their further incorporating with BiOBr photocatalysts. Till now, there is an increasing trend to prepare carbonaceous materials using the cheap, readily attainable and environmental friendly biomass as starting materials<sup>33,34</sup>. The biomass-derived carbonaceous aerogels were traditionally obtained via a well-established hydrothermal carbonization (HTC) under mild conditions<sup>27,34-37</sup>. The carbonaceous aerogel has not only the functional characteristics of carbon aerogel, but also the peculiar features such as containing abundant functional groups, surface hydrophilicity, excellent adsorption capacity and chemical reactivity.

Herein, we described a novel winter melon-derived ultralight carbonaceous aerogel support modified with flower-like BiOBr through a facile solvothermal approach as a highly efficient photocatalyst for the degradation of rhodamine B (RhB) under visible light. The 3D porous carbonaceous aerogel was firstly synthesized by HTC process using winter melon as raw material and then modified by 2,2,6,6-tetramethylpiperidinoxy (TEMPO)-mediated oxidation. Finally, flower-like BiOBr was embedded in the oxidized winter melon-derived carbonaceous aerogel (OWMCA) by a simple alcohol-thermal method. The resulting BiOBr modified OWMCA (BOB@OWMCA) composite displayed excellent adsorption capacity and superior degradation performance for organic dyes. Furthermore, BOB@OWMCA composite with a relative light weight can float on water surface as a monolithic photocatalyst, providing great convenience for collection and separation.

## Experimental Section

### Materials

All the chemicals were of analytic purity and used without further purification. Fresh winter melons were purchased from a local supermarket. Bismuth nitrate hydrate ( $\text{Bi}(\text{NO}_3)_3 \cdot 5\text{H}_2\text{O}$ ), ethylene glycol, isopropanol, sodium bromide (NaBr), dehydrated alcohol, sodium hypochlorite (NaClO) solution, hydrochloric acid (HCl) and sodium hydroxide (NaOH) were purchased from Sinopharm Chemical Reagent Co., Ltd (China). 2,2,6,6-tetramethyl-piperidiny-1-oxyl (TEMPO, 98%) was purchased from Sigma Aldrich.



**Scheme 1** Schematic diagram of the synthesis of BOB@OWMCA hybrid aerogel.

### Preparation of winter melon-derived carbonaceous aerogel (WMCA)

The WMCA was prepared through HTC process according to the previous report<sup>25</sup>. After removing the rind, soft pulp and seeds, the fresh winter melon was carefully cut into the appropriate squares using a sharp knife and put into Teflon-lined stainless steel autoclave. Then the autoclave was sealed and maintained at 180 °C for 10 h. After cooling down to room temperature, the as-obtained carbonaceous hydrogel was immersed into hot water at 60 °C for 2 days to remove the soluble impurities. Finally, ultralight WMCA was obtained after freeze-drying of carbonaceous hydrogel at -45 °C for 24 h.

### Preparation of TEMPO-mediated oxidized winter melon carbonaceous aerogel (OWMCA)

WMCA was modified according to a previous procedure described by Lin et al<sup>38</sup>. First, TEMPO and NaBr in a given ratio were dissolved in deionized water with stirring for 10 min. Then the WMCA and a certain amount of NaClO solution were successively added into the mixed dispersion, followed by adjusting pH value to 10 with NaOH solution addition. The oxidizing reaction was terminated after 6 h, followed by adjusting pH value to 7 with hydrochloric acid addition. Subsequently, the oxidized winter melon carbonaceous hydrogel was thoroughly washed by deionized water and dehydrated alcohol, and freeze-dried at -45 °C for 24 h to obtain OWMCA.

### Preparation of BiOBr modified TEMPO-mediated oxidized winter melon carbonaceous aerogel (BOB@OWMCA)

BOB@OWMCA composite was prepared via a solvothermal synthesis. First, the BiOBr precursor solution was obtained by dissolving  $\text{Bi}(\text{NO}_3)_3 \cdot 5\text{H}_2\text{O}$  and NaBr with a required amount in a two-component solvents mixed with ethylene glycol and isopropanol. After the OWMCA was immersed into the solution under stirring at the room temperature for 30 min, the mixtures was subsequently transferred into 100 mL Teflon-lined stainless steel autoclave with 80% volume filled. Herein, the mole ratio of  $\text{Bi}(\text{NO}_3)_3 \cdot 5\text{H}_2\text{O}$  and NaBr was selected as 1:1, and the weight ratios of BiOBr (in theory) to OWMCA varied with 2.5, 5, 10 and 20. The autoclave was sealed and heated at 160 °C for 12 h. Thus the BOB@OWMCA composite was ultimately assembled by washing with deionized water for several times and subsequently freeze-dried at -45 °C for 24 h. The schematic diagram was shown in Scheme 1.

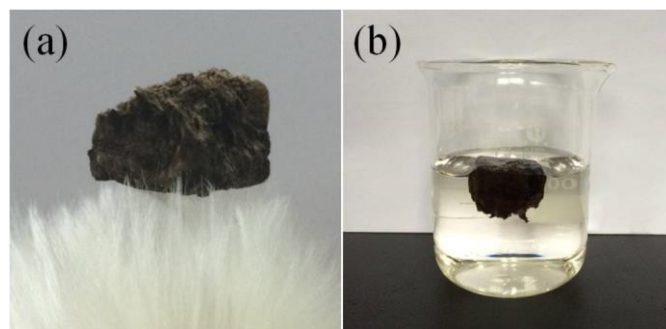


**Figure 1** Digital photographs of OWMCA monolith standing on feathers (a) and floating beneath water surface (b).

### Preparation of BiOBr modified winter melon carbonaceous aerogel (BOB@WMCA)

As a comparison, BOB@WMCA was synthesized by the similar solvothermal method with WMCA as a support.

#### Characterization

Surface morphologies of all samples were examined by scanning electron microscopy (SEM, S-4800, Hitachi). The structure was characterized through Fourier transform infrared spectroscopy (FTIR, AVATAR370, Nicolet) with the spectral width ranging from 4000 to 400  $\text{cm}^{-1}$  by grinding KBr as transparent pellets. X-ray diffraction (XRD, D/max-2500, Japan) patterns were measured in the range from 5° to 75° with Ni-filtered Cu K $\alpha$  radiation ( $V = 50$  kV,  $I = 80$  mA) at a scanning rate of 8 °/min. Raman spectra were examined at room temperature using Raman spectroscopy (inVia-reflex, Renishaw). The optical properties were measured by UV-vis spectrophotometer (UV-2501PC, Shimadzu). N<sub>2</sub> adsorption-desorption isotherms were measured on a Quantachrome instrument (ASIQCU02U-5) at 77 K. The Brunauer-Emmett-Teller (BET) was utilized to calculate the specific surface area ( $S_{\text{BET}}$ ) based on the N<sub>2</sub> adsorption branches.

#### Photodegradation test

Liquid-phase photodegradation of RhB was carried out at room temperature in a self-designed quartz tube (3 cm ( $\varphi$ )  $\times$  12 cm ( $L$ )) equipped containing 52.0 mg catalysts and 50.0 mL 10.0 mg/L RhB aqueous solution. As a comparison, pure BiOBr was submerged below the water surface and remained stationary under same conditions. After reaching adsorption equilibrium in the dark for 2 h, the photodegradation reaction was initiated by irradiating the reactor with four fluorescent lamps ( $\lambda = 400\text{--}800$  nm, 14 W, Royal Dutch Philips Electronics Ltd), with a light intensity of 10.0  $\text{mW}/\text{cm}^2$  (measured by a radiometer, LP-3 A, Beijing Wuke Photoelectric Technique Co., Ltd) by adjusting the distance between the lamp and reactor. The concentration of RhB left in the solution was determined by the UV-vis spectroscopy at given time intervals. The results were checked by repeating the experiment for three times within a permitted error limit ( $\pm 5\%$ ).

## Results and Discussion

3D sponge-like WMCA was surface modified by grafting carboxyl groups via a TEMPO-mediated oxidation to increase the possibility for further functionalization. Both WMCA and OWMCA show porous multilayer network architectures (Figure S1), which enable them to be excellent 3D scaffold.

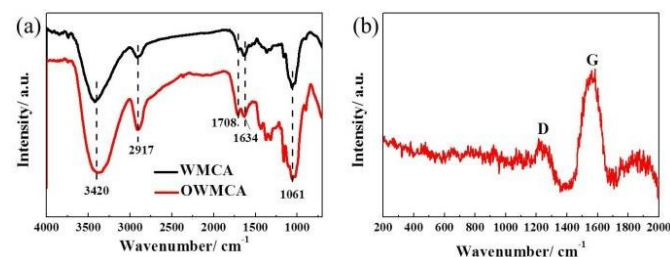
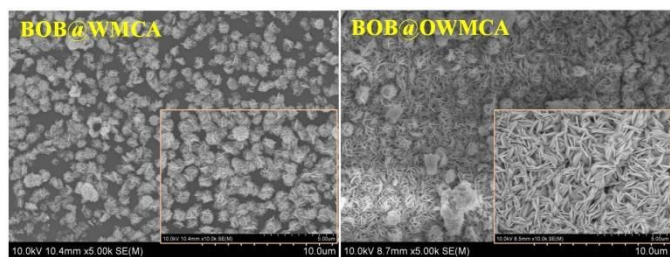


Figure 2 FT-IR spectra of WMCA and OWMCA (a) and Raman spectrum of OWMCA (b).

Figure 1a shows that the as-prepared OWMCA monolith with dark brown color can easily stand on a bundle of erected feathers. The ultra-lightweight property will make it a promising platform to load a range of functional nanomaterials for diverse applications. The OWMCA with a mass density of 17.7  $\text{mg}/\text{cm}^3$  can float beneath the surface after immersing into water (as shown in Figure 1b), suggesting the porous OWMCA was endowed with extremely hydrophilicity, ultralight weight and high adsorption performance. In addition, the OWMCA monolith can easily be divided into arbitrary desired shapes to match the requirement of applications (Figure S2).

The surface functional groups of the resultant samples are identified by FT-IR spectroscopy as shown in Figure 2a. The characteristic signals located at 3420  $\text{cm}^{-1}$  and 2917  $\text{cm}^{-1}$  are attributed to stretching vibration of -OH groups and stretching vibrations of C-H, respectively. The bands at 1634  $\text{cm}^{-1}$  is attributed to the C=O or C=C stretching vibrations, probably resulting from furanic or aromatic groups formed by polymerization-polycondensation reactions during HTC process<sup>28,39,40</sup>. After the TEMPO-mediated oxidation, the obvious change for OWMCA is the enhancement of band at 1708  $\text{cm}^{-1}$  attributed to the stretching vibration of free carboxyl groups C=O coming from -COOH in comparison with WMCA<sup>38</sup>, suggesting the increasing amount of C=O group formed by oxidization of OH band. The results indicate that the surface of OWMCA is rich in functional groups, which enhance the accessibility for further reaction with other guest materials. The Raman spectrum is also determined to evaluate the disordered structure of OWMCA (Figure 2b). The board and strong band at 1561  $\text{cm}^{-1}$  (G) is attributed to first-order scattering of the E<sub>2g</sub> phonon of the sp<sup>2</sup> carbon domains in a two-dimensional hexagonal lattice, however the band at 1242  $\text{cm}^{-1}$  (D) corresponds to disorder-induced mode associate with structure defects and imperfections<sup>40,41</sup>. Therefore, the intensity ratio of D and G bands ( $I_{\text{D}}/I_{\text{G}}$ ) can reflect the quality of graphitic structures. The calculated  $I_{\text{D}}/I_{\text{G}}$  ratio of OWMCA is about 0.335, indicating that a number of disordered structures are generated. It is probably due to the presence of the isolated double bond (C=O and C=C) on the surface of OWMCA or the TEMPO oxidation reaction induced an increase of defects in the carbon network.

Benefiting from the surface functional groups and the defects in carbon structure, the porous multilayer networks provide an additional surface for the heterogeneous nucleation of BiOBr, thus BiOBr can easily be introduced into the active sites of the OWMCA according to the typical solvothermal process. The digital photo of BOB@OWMCA (Figure S3) shows the color turned from dark brown to yellow due to the incorporation of BiOBr. The surface morphologies of BOB@WMCA and BOB@OWMCA are presented in Figure 3, respectively. It is obvious that the surface of WMCA is covered by well-dispersed 3D flower-like BiOBr microspheres with diameters of 0.5-1  $\mu\text{m}$  (Figure S4) constructed by numerous 2D interlaced nanosheets. Interestingly, highly uniform and contact flower-like BiOBr with massive nanosheets coated on the whole



**Figure 3** SEM images of BOB@WMCA and BOB@OWMCA with the same weight ratio of BiOBr (inset: the corresponding high magnification).

OWMCA surface is clearly observed. The difference between BOB@WMCA and BOB@OWMCA is contributed that the active sites generated from TEMPO oxidation reaction provide more opportunities for the crystal growth and immobilization of BiOBr nucleus. It is well acknowledged that the BiOBr easily forms nanosheets and further self-assemble to hierarchical microspheres<sup>4</sup>. But the sufficient contact area of OWMCA improves the homogeneous distribution of BiOBr nanosheets, meanwhile inhibits the self-assembly of BiOBr nanosheets to form excessive microspheres, as shown in the high magnification SEM images (insets in Figure 3). On the basis of the well dispersibility of BiOBr nanosheets with high-loading attached onto the surface of OWMCA, the as-synthesized BOB@OWMCA hybrid material will exhibit the synergetic properties of BiOBr photocatalyst and OWMCA support to strengthen photodegradation activity.

Figure 4 shows the SEM images of BOB@OWMCA with the different ratios of BiOBr to OWMCA varied from 2.5:1, 5:1, 10:1 to 20:1 (Table 1). It can be clearly observed that all BOB@OWMCA maintain the monolithic architectures of original OWMCA, and display well-dispersed BiOBr with relatively uniform size distribution is loaded on the surface of OWMCA. With the increasing ratio of BiOBr to OWMCA, the higher surface accumulation and even multi-layer agglomerates of BiOBr appeared on the surface of OWMCA, especially for BOB@OWMCA-10 and BOB@OWMCA-20.

The corresponding densities of BOB@OWMCA composites are summarized in Table 1, the densities of BOB@OWMCA exhibited an increasing trend with the increasing amount of BiOBr, much higher than pure OWMCA. The surface area is one of the important characteristics for photocatalytic properties, which can provide more opportunities for the photocatalysts to touch with light and reactants, resulting in the enhancement of photocatalytic activity. The  $S_{\text{BET}}$  of samples are investigated by  $\text{N}_2$  adsorption–desorption isotherms, as shown in Figure S5. The isotherms of BOB@OWMCA with the different ratios of BiOBr to OWMCA can be categorized as type IV with the distinct hysteresis loop at about  $p/p_0 = 0.5\text{--}1.0$ , indicative of the mesoporous structure resulting from the OWMCA and the self-assembly of BiOBr microspheres<sup>4</sup>. The  $S_{\text{BET}}$  of OWMCA, BOB, BOB@OWMCA and BOB@WMCA are summarized in Table 1. All the BOB@OWMCA samples show larger  $S_{\text{BET}}$  than pure OWMCA and BOB, while BOB@WMCA exhibits much lower  $S_{\text{BET}}$  than others probably due to the inadequate linking between BOB and WMCA.

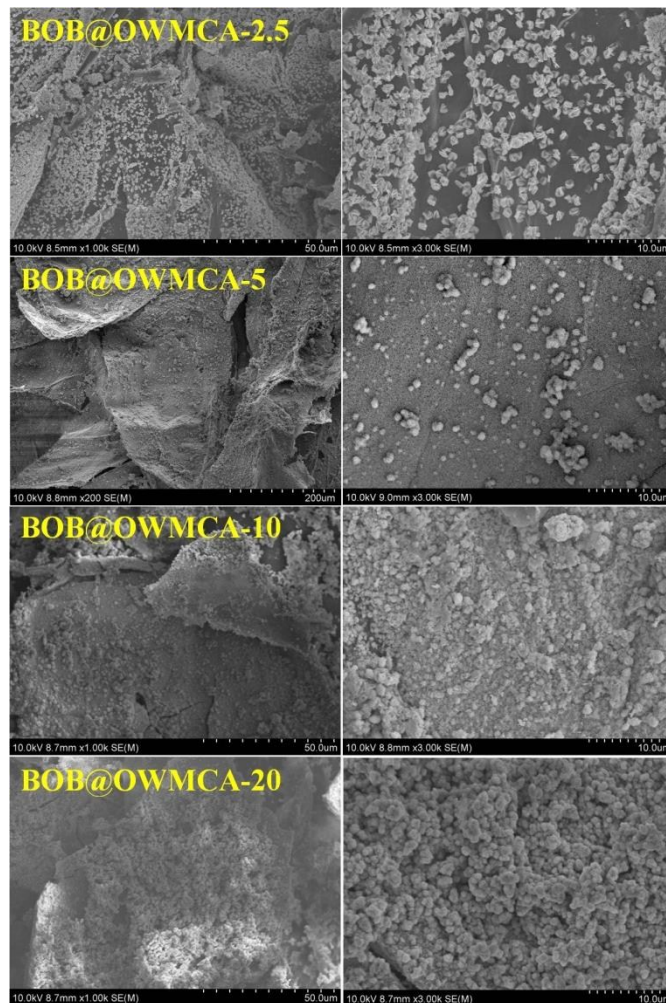


**Figure 4** SEM images of BOB@OWMCA with the different ratios of BiOBr to OWMCA (2.5:1, 5:1, 10:1 and 20:1). Left: the low magnification; Right: the high magnification.

Figure 5 compares XRD patterns of BOB, OWMCA and BOB@OWMCA-20. It can be found that all the peaks of BOB are assigned to the typical tetragonal structure (JCPDS No. 09-0393). The OWMCA exhibits the typical cellulose I structure with the broad characteristic peaks located at  $2\theta = 15^\circ$ ,  $22^\circ$  and  $35^\circ$ . The peaks at  $2\theta = 38^\circ$ ,  $44^\circ$  and  $65^\circ$  can be attributed to the presence of impurities from the origin winter melon. It is obviously observed that BOB@OWMCA-20 exhibits the typical

Table 1 Structure parameters and photoactivities of different samples.

Sample	Weight ratio	$\rho$ (mg/cm <sup>3</sup> )	$S_{\text{BET}}$ (m <sup>2</sup> /g)	Photodegradation rate (%)
OWMCA	/	17.7	30.6	46.2
BOB@OWMCA-2.5	2.5:1	44.1	/	81.0
BOB@OWMCA-5	5:1	48.4	36.7	92.0
BOB@OWMCA-10	10:1	53.2	40.0	95.2
BOB@OWMCA-20	20:1	63.9	52.6	100
BOB	/	/	35.9	65.9
BOB@WMCA-10	10:1	/	16.4	/

Reaction conditions: 52.0 mg catalyst, 50.0 mL 10.0 mg/L RhB aqueous solution, room temperature reaction, four fluorescent lamps ( $\lambda = 400\text{--}800$  nm, 14 W), reaction time = 120 min.

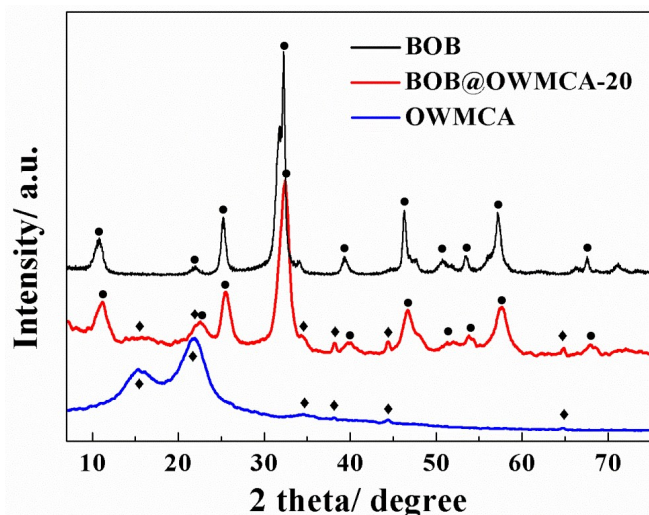


Figure 5 XRD patterns of BOB, OWMCA and BOB@OWMCA-20.

diffraction peaks of both BOB and OWMCA. In addition, a red shift is detected from all of the BOB peaks in BOB@OWMCA-20 diffraction patterns, representing the change of lattice spacing of BiOBr crystal. The results indicate that BiOBr was bound to OWMCA by the ways of physical deposition and chemical bonding. The strong chemical interaction between BiOBr and OWMCA enhance the stability and recyclability.

The optical properties of OWMCA and BOB@OWMCA were measured according to UV-vis diffuse reflection spectra. As shown in Figure 6, all the BOB@OWMCA samples reveal much stronger adsorption than OWMCA in the wavelength range from 210 to 710 nm, implying that BiOBr plays the key role in the light adsorption. Therefore, with the increasing ratio of BiOBr to OWMCA from 5:1 to 20:1, BOB@OWMCA shows higher absorption in UV and visible light regions. Similar to the previous report<sup>42</sup>, the flower-like BiOBr microspheres assembled by nanosheets provide many spaces for the entry of light, resulting in the light multi-reflection, which is beneficial for the improvement of photodegradation property.

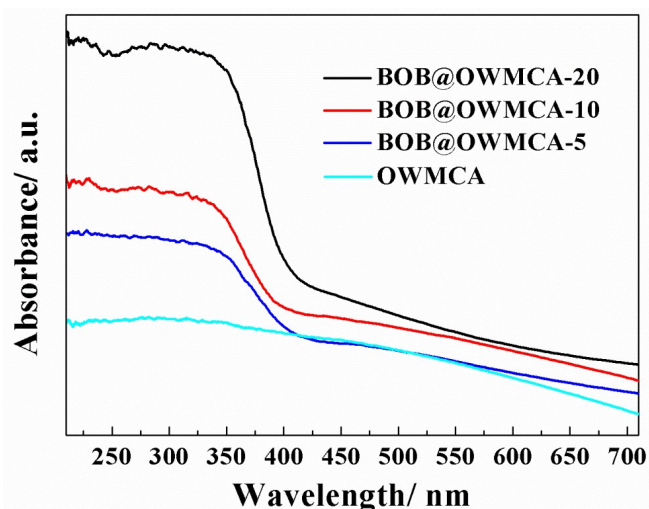


Figure 6 UV-vis diffuse reflection spectra of OWMCA and BOB@OWMCA composites with different ratios of BiOBr to OWMCA (5:1, 10:1 and 20:1).

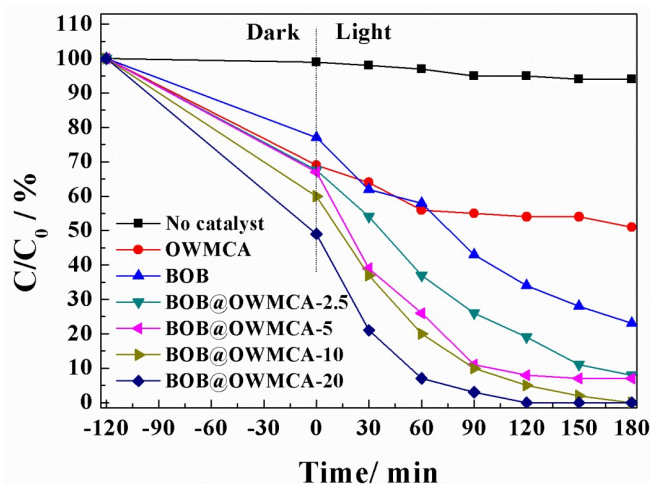
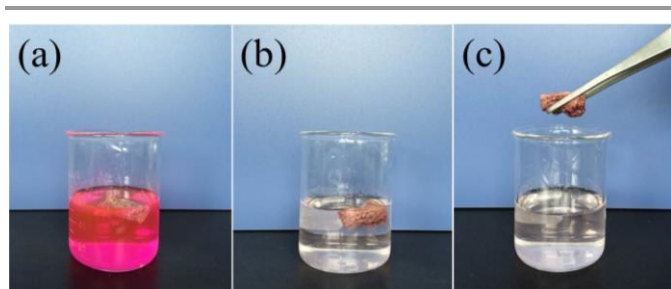


Figure 7 Reaction process for photodegradation of RhB with different catalysts.  $C_0$  and  $C$  referred to the initial RhB concentration and the RhB concentration determined at different reaction time, respectively. Reaction conditions: 52.0 mg catalyst, 50.0 mL RhB aqueous solution (10.0 mg/L), room temperature reaction, four fluorescent lamps ( $\lambda = 400\text{--}800$  nm, 14 W).

The photodegradation of RhB under visible light irradiation can be used to evaluate the photocatalytic activity of BOB@OWMCA shown in Figure 7. As comparison, a blank experiment was firstly carried out in the absence of photocatalyst, and only about 5% RhB was decomposed under visible light irradiation, thus the self-photodegradation of RhB could be negligible during the photocatalysis process. The adsorption and desorption of RhB on photocatalysts reach the equilibrium after 120 min in the dark. Compared with the blank experiment, degradation rates ( $C/C_0$ ) are accelerated in the presence of photocatalysts. It can be found that OWMCA exhibits a much stronger RhB adsorption than BiOBr in the dark, attributed to the strong hydrophilicity and the face-to-face oriented adsorption between RhB and the functional groups<sup>43</sup>. On the contrary, BiOBr displays a much higher degradation rate of RhB with prolonging time than OWMCA under the visible light irradiation, ascribed to the efficient light multi-reflection and high photocatalytic activity of flower-like BiOBr nanosheets. The hierarchical structure endows fast charge transport, resulting in lower recombination rates compared to particulate nanomaterials<sup>31</sup>.

It can be deduced that the BOB@OWMCA comprising of OWMCA and BiOBr simultaneously play the synergistic roles in the adsorption and photodegradation of RhB. Although there may be a certain amount of BiOBr inside the cavity of OWMCA, the multi-reflection of light within the interior cavity of OWMCA still leads to an increase of light-harvesting efficiency of the attached BiOBr in porous surface<sup>42</sup>. Therefore, the enhanced photocatalytic activity with the increasing ratios of BiOBr to OWMCA is attributed to the larger  $S_{\text{BET}}$  and higher capacity of capture visible light via light multi-reflections. The  $C/C_0$  rates of RhB at the reaction time of 120 min for different catalysts are summarized in Table 1. Encouraged by the synergistic effect of adsorption and photocatalysis, the degradation rates of RhB with the presence of BOB@OWMCA are further accelerated. BOB@OWMCA-2.5, BOB@OWMCA-5,



**Figure 8** Digital photographs of the photodegradation of RhB before (a) and after (b,c) visible light irradiation using the as-prepared BOB@OWMCA-10.

BOB@OWMCA-10, BOB@OWMCA-20 degraded 81.0%, 92.0%, 95.2% and 100% of RhB in 120 min under visible light irradiation, respectively.

Of importance here is that the BOB@OWMCA composite as a monolithic photocatalyst has a remarkable advantage for facile separation from the reaction system. As shown in Figure 8a and b, BOB@OWMCA composite maintains high shape stability during the whole degradation process of RhB. Unlike the conventional filtration or centrifugation separation process for granular BiOBr photocatalyst, the floating BOB@OWMCA composite can be easily collected for separation (Figure 8c). After removal of the absorbed RhB by a simple squeezing process, the adsorption and photodegradation capacity of BOB@OWMCA were decreased (not shown), which can be attributed to the residual RhB absorbed inside OWMCA and the collapse of 3D porous structure. In fact, molecules of RhB adsorbed onto the BOB@OWMCA composite should be easily removed by further irradiating with fluorescent lamps ( $\lambda = 400\text{--}800\text{ nm}$ ) in the solid conditions for a prolonged time.

## Conclusions

In summary, a novel BiOBr decorated carbon-based aerogel composite photocatalyst was successfully assembled via a facile solvothermal method using TEMPO-mediated oxidized winter melon carbonaceous aerogel (OWMCA) as a support. The active functional groups and defects on the surface of OWMCA were advantageous to the growth and immobilization of BiOBr, resulting in a homogenous distribution of BiOBr nanosheets with high loading on the surface of OWMCA. Due to the ultralight weight and high specific surface area, OWMCA support provided an efficient platform to strengthen the adsorption capability and photodegradation activity for organic dye (RhB). The as-prepared BOB@OWMCA composite with a proper ratio presented an RhB removal efficiency of almost 100% under 120 min under visible light irradiation. Furthermore, the BOB@OWMCA was easily collected and separated from the reaction system. This strategy of anchoring photocatalyst on low-cost biomass-based support will promote the scale-up synthesis of semiconductor visible light photocatalysts that combine enhanced photodegradation activities with easy separation property used in practical application.

## Acknowledgements

This work was financially sponsored by Natural Science Foundation of Shanghai (13ZR1415100, 15ZR1415100). We are also grateful to Instrumental Analysis & Research Center of Shanghai University.

## Notes and references

- Z. G. Zou, J. H. Ye, K. Sayama and H. Arakawa, *Nature*, 2001, **414**, 625.
- J. G. Yu and X. X. Yu, *Environ. Sci. Technol.* 2008, **42**, 4902.
- C. C. Shen, Q. Zhu, Z. W. Zhao, T. Wen, X. Wang and A. W. Xu, *J. Mater. Chem. A* 2015, **3**, 14661.
- Y. N. Huo, J. Zhang, M. Miao and Y. Jin, *Appl. Catal. B* 2012, **111–112**, 334.
- J. Jiang, K. Zhao, X. Y. Xiao and L. Z. Zhang, *J. Am. Chem. Soc.* 2012, **134**, 4473.
- J. X. Xia, S. Yin, H. M. Li, H. Xu, Y. S. Yan, and Q. Zhang, 2011, **27**, 1200.
- H. J. Zhang, Y. X. Yang, Z. Zhou, Y. P. Zhao and L. Liu, *J. Phys. Chem. C* 2014, **118**, 14662.
- H. Li, J. Shang, Z. H. Ai, and L. Z. Zhang, *J. Am. Chem. Soc.* 2015, **137**, 6393.
- L. L. Li, L. H. Ai, C. H. Zhang and J. Jiang, *Nanoscale* 2014, **6**, 4627.
- J. Xu, W. Meng, Y. Zhang, L. Li and C. S. Guo, *Appl. Catal. B* 2011, **107**, 355.
- J. Y. Xiong, Q. S. Dong, T. Wang, Z. B. Jiao, G. X. Lu and Y. P. Bi, *RSC Adv.* 2014, **4**, 583.
- H. W. Huang, X. Han, X. W. Li, S. C. Wang, P. K. Chu and Y. H. Zhang, *ACS Appl. Mater. Interfaces* 2015, **7**, 482.
- J. Cao, B. Y. Xu, B. D. Luo, H. L. Lin and S. F. Chen, *Catal. Comm.* 2011, **13**, 63.
- Z. S. Liu, H. S. Ran, B. T. Wu, P. Z. Feng and Y. B. Zhu, *Colloids Surf. A* 2014, **452**, 109.
- K. Li, H. B. Zhang, Y. P. Tang, D. W. Ying, Y. L. Xu, Y. L. Wang and J. P. Jia, *Appl. Catal. B* 2015, **164**, 82.
- R. Mitchell, R. Brydson and R. E. Douthwaite, *Phys. Chem. Chem. Phys.* 2015, **17**, 493.
- E. L. Cuellar, A. M. Cruz, N. C. Torres and J. O. Cortez, *Catal. Today* 2015, **252**, 2.
- S. M. Wang, P. Liu, X. X. Wang and X. Z. Fu, *Langmuir* 2005, **21**, 11969.
- S. W. Zhang, J. X. Li, M. Y. Zeng, G. X. Zhao, J. Z. Xu, W. P. Hu and X. K. Wang, *ACS Appl. Mater. Interfaces* 2013, **5**, 12735.
- S. W. Zhang, J. X. Li, X. K. Wang, Y. S. Huang, M. Y. Zeng and J. Z. Xu, *J. Mater. Chem. A* 2015, **3**, 10119.
- C. Li and G. Q. Shi, *Adv. Mater.* 2014, **26**, 3992.
- S. Nardecchia, D. Carriazo, M. L. Ferrer, M. C. Gutiérrez and F. D. Monte, *Chem. Soc. Rev.* 2013, **42**, 794.
- L. H. Yu, N. Brun, K. Sakaushi, J. Eckert and M. M. Titirici, *Carbon*, 2013, **61**, 245.
- L. P. Wang, C. Schütz, G. Salazar-Alvarez and M. M. Titirici, *RSC Adv.* 2014, **4**, 17549.
- G. X. Zhao, X. B. Huang, X. K. Wang, P. Connor, J. X. Li, S. W. Zhang and J. T. S. Irvine, *J. Mater. Chem. A* 2015, **3**, 297.
- W. Chen, R. B. Rakhi, L. B. Hu, X. Xie, Y. Cui and H. N. Alshareef, *Nano Lett.* 2011, **11**, 5165.
- Y. Q. Li, Y. A. Samad, K. Polychronopoulou, S. M. Alhassan and K. Liao, *ACS Sustainable Chem. Eng.* 2014, **2**, 1492.
- H. C. Bi, X. Huang, X. Wu, X. H. Cao, C. L. Tan, Z. Y. Yin, X. H. Lu, L. T. Sun and H. Zhang, *Small* 2014, **10**, 3544.
- W. J. Liu, J. Y. Cai and Z. H. Li, *ACS Sustainable Chem. Eng.* 2015, **3**, 277.
- A. K. Geim, *Science* 2009, **324**, 1530.

- 31 G. Lui, J. Y. Liao, A. S. Duan, Z. S. Zhang, M. Fowler and A. P. Yu, *J. Mater. Chem. A* 2013, **1**, 12255.
- 32 J. Liang, Y. Zheng, J. Chen, J. Liu, D. Hulicova-Jurcakova, M. Jaroniec and S. Z. Qiao, *Angew. Chem. Int. Ed.* 2012, **51**, 3892.
- 33 H. C. Bi, Z. Y. Yin, X. H. Cao, X. Xie, C. L. Tan, X. Huang, B. Chen, F. T. Chen, Q. L. Yang, X. Y. Bu, X. H. Lu, L. T. Sun and H. Zhang, *Adv. Mater.* 2013, **25**, 5916.
- 34 X. L. Wu, T. Wen, H. L. Guo, S. B. Yang, X. K. Wang and A. W. Xu, *ACS Nano* 2013, **7**, 3589.
- 35 N. Brun, P. Osiceanu and M. M. Titirici, *ChemSusChem*, 2014, **7**, 397.
- 36 B. Hu, K. Wang, L. H. Wu, S. H. Yu, M. Antonietti and M. M. Titirici, *Adv. Mater.* 2010, **22**, 813.
- 37 M. M. Titirici, R. J. White, C. Falco and M. Sevilla, *Energy Environ. Sci.* 2012, **5**, 6796.
- 38 N. Lin, C. Bruzzese and A. Dufresne, *ACS Appl. Mater. Interfaces* 2012, **4**, 4948.
- 39 Y. Jin, H. Y. Chen, M. H. Chen, N. Liu and Q. W. Li, *ACS Appl. Mater. Interfaces* 2013, **5**, 3408.
- 40 Y. M. Ren, Q. Xu, J. M. Zhang, H. X. Yang, B. Wang, D. Y. Yang, J. H. Hu and Z. M. Liu, *ACS Appl. Mater. Interfaces* 2014, **6**, 9689.
- 41 S. W. Lee, S. M. Bak, S. W. Lee, C. Jaye, D. A. Fischer, B. K. Kim, X. Q. Yang, K. W. Nam and K. B. Kim, *J. Phys. Chem. C* 2014, **118**, 2834.
- 42 H. X. Li, Z. F. Bian, J. Zhu, D. Q. Zhang, G. S. Li, Y. N. Huo, H. Li and Y. F. Lu, *J. Am. Chem. Soc.* 2007, **129**, 8406.
- 43 L. L. Zhang, Z. G. Xiong and X. S. Zhao, *ACS Nano* 2010, **4**, 7030.